Melting–Crystallization and Premelting Properties of $NaNO_3$–KNO_3. Enthalpies and Heat Capacities

Derek J. Rogers and George J. Janz*

Cogswell Laboratory, Rensselaer Polytechnic Institute, Troy, New York 12181

Data for the enthalpies for the solid-state transition and for melting, and the heat capacities, gained by the method of DSC calorimetry, are reported for the equimolar composition of $NaNO_3$–KNO_3 (drawsalt). The measurements of the melting–crystallization properties were extended to span the complete composition range of this binary system, and the results are correlated with the solidus–liquidus lines of the phase diagram for this system. A limited series of measurements were also undertaken on the influence of prolonged exposure to ambient air atmosphere of the drawsalt while in the molten state (at ~600 °C), and these results are also reported.

Introduction

In some of the advanced concepts for thermal energy storage from the sun and subsequent electric power (*1*, *2*), molten salts have been proposed as candidate materials both as high-temperature heat-transfer fluids and as media for sensible heat storage. The binary nitrate system $NaNO_3$–KNO_3 is one of the principal candidate systems thus short-listed. The data status for this system was part of a physical properties data compilation relevant to energy storage reported elsewhere in 1979 (*3*), and it is sufficient to note that the fusion properties and heat capacity data appeared to be limited to two studies, Marchidan and Telea (*4*) and Voskresenskaya et al. (*5*), respectively.

Two additional investigations for this system have been reported since the above work, namely, Nguyen-Duy and Dancy (*6*) and Carling (*7*), both for fusion properties and heat capacity measurements, and both limited to the equimolar mixture referred to as drawsalt. Inspection of the results indicates that the values of heats of fusion reported are respectively 2.95 (*4*), 2.53 (*5*), 2.50 (*6*), and 2.44 (*7*) kcal mol^{-1} and that values for heat capacities differ by more than 20% at the lower temperature limit (~510 K) (*5*, *7*) and, furthermore, also differ markedly in the slopes of the temperature dependence of the heat capacity data (*5*, *7*). The results reported in the present communication are based on work that was in progress when the situation was thus perplexed. The measurements in progress were thus extended to encompass the composition range required to define the complete binary system. A limited series of measurements were also undertaken to investigate the influence of exposure of the molten nitrates to ambient atmospheric "air" for prolonged periods, and these results are also reported herewith.

Experimental Section

All samples were prepared in the DSC capsules by weighing in directly the $NaNO_3$ and KNO_3 in the amounts required for each composition. The nitrates were highest-purity grades (99.999% purities) and were used without further pretreatment except for oven drying (10^{-4} torr, ~150 °C) to remove ambient atmospheric moisture and air. The small mass measurement facility (Cahn electrobalance) and the DSC capsule crimp-press were kept in a dry N_2 atmosphere so that all weighing for the in-capsule samples preparation, and the hermetic crimp seal, could be accomplished without reexposure to atmospheric moisture and air. Before the calorimetric measurements, the encapsuled samples were thermally cycled, repeatedly from ~50 °C, through the melting–crystallization transition, and to ~340 °C to achieve well-mixed and homogeneous compositions for the mixtures. Generally, approximately two to five thermal cycles were required in this step. Compositions from 5 to 90 mol % $NaNO_3$ were thus prepared for the enthalpy and heat capacity measurements.

To investigate the influence of prolonged exposure of the nitrates in the molten state to ambient atmospheric air, we modified the preparative technique so that two aliquots of the same specimen could be used for the calorimetric measurements, to compare the properties before and after exposure. For this purpose, the mixtures were prepared in ~6-g amounts and premelted in air at ~250 °C to attain homogeneity of composition. The samples were cooled, and aliquots were removed for characterization of the properties. The remainders were heated in platinum crucibles to ~600 °C, open to atmospheric air, and thus maintained for ~7 days, prior to further calorimetric measurements. All encapsulations were made with the small mass measurement facility and crimp-press already described.

The calorimetric facility centered around a Perkin-Elmer Model-2 DSC instrument, computer-aided through the Laboratory Microsystems digital control system for automated data acquisition, base-line corrections, data analysis, and graphics for enthalpy and heat capacity measurements. The accuracy limits, established through energy calibration cross-checks with three metals (indium, tin, and lead) and two salt systems (KNO_3 and LiCl–KCl eutectic) were as follows: ±0.5 °C; enthalpies, ±1.0%; and heat capacities, ±2.0%.

For $NaNO_3$–KNO_3 series, the measurements were made with the instrument heating and cooling rates set at 10 °C min^{-1}, and the N_2 sweep rate through the DSC assembly was ~20 cm^3 min^{-1}. The heat capacity data acquisition was programmed in overlapping 50 °C temperature increments from the lower to the upper temperature limits in this series.

Results and Discussion

Melting temperatures were determined by following the procedures noted below. Thus, for the isothermally melting materials, namely, $NaNO_3$, KNO_3, and the minimum-melting mixture, the T_m values were obtained by extrapolating the leading edge of the endotherm to the point of base-line intersection. The slope of the leading edge is a function of the thermal lag of the DSC calorimeter for isothermally melting materials. This is in contrast to nonisothermally melting systems, such as the intermediate compositions in the $NaNO_3$–KNO_3 systems, the equimolar composition being excepted. For such systems the slowness of the melting process overrides the thermal lag (above) so that the temperature range for the melting process may now be gained from the base-line intersections of the leading and trailing edges, respectively, and the apparent "melting point", i.e., the point of maximum rate of melting, is taken as the deepest point of the endotherm. For such mixtures, the completion of the melting process, however, is defined as the point of return from the endotherm to the base line. For mixtures also, the measured enthalpies and heat capacities

0021-9568/82/1727-0424$01.25/0

Table I. Enthalpies of Solid-State Transitions and Melting for $NaNO_3$–KNO_3

A. Solid State Transition Temperatures and Enthalpies

($NaNO_3$), mol %	mol wt,[b] g	T_{range}, K	T_{tr}, K	ΔH_{tr},[a] cal mol^{-1}
0	101.10	400-410	403	1213
5	100.30	381-405	399	1322
13	99.01	373-403	391	1238
25	97.08	378-405	384	1169
40	94.66	366-397	378	786
46	93.70	373-390	383	765
50	93.06	378-404	386	751
60	91.45	377-395	383	544
64	90.80	378-393	384	462
75	89.03	375-400	382	306
90	86.62	375-410	384	135
100	85.01	450-560	549	225

B. Melting Transition Temperatures and Enthalpies

($NaNO_3$), mol %	mol wt,[b] g	T_{range}, K	T_{tr}, K	ΔH_{fus},[a] kcal mol^{-1}
0	101.10	[c]	608	2.39
5	100.30	550-599	575	2.26
13	99.01	494-581	538	2.16
25	97.08	492-545	519	2.10
40	94.66	484-509	497	2.16
46	93.70	484-505	495	2.19
50	93.06	[c]	493	2.24
60	91.45	486-509	498	2.40
64	90.80	488-518	503	2.46
75	89.03	492-540	516	2.69
90	86.62	472-567	520	3.06
100	85.01	[c]	579	3.69

[a] For conversion to SI units, 1 cal = 4.184 J. [b] For mixtures, the "mol wt" is calculated from the molecular weights of $NaNO_3$ and KNO_3 and the principles of mole fraction additivity. [c] These three compositions (0, 50, and 100 mol % $NaNO_3$) melt isothermally; for all others, the T limits indicate the solidus and liquidus temperatures (see phase diagram).

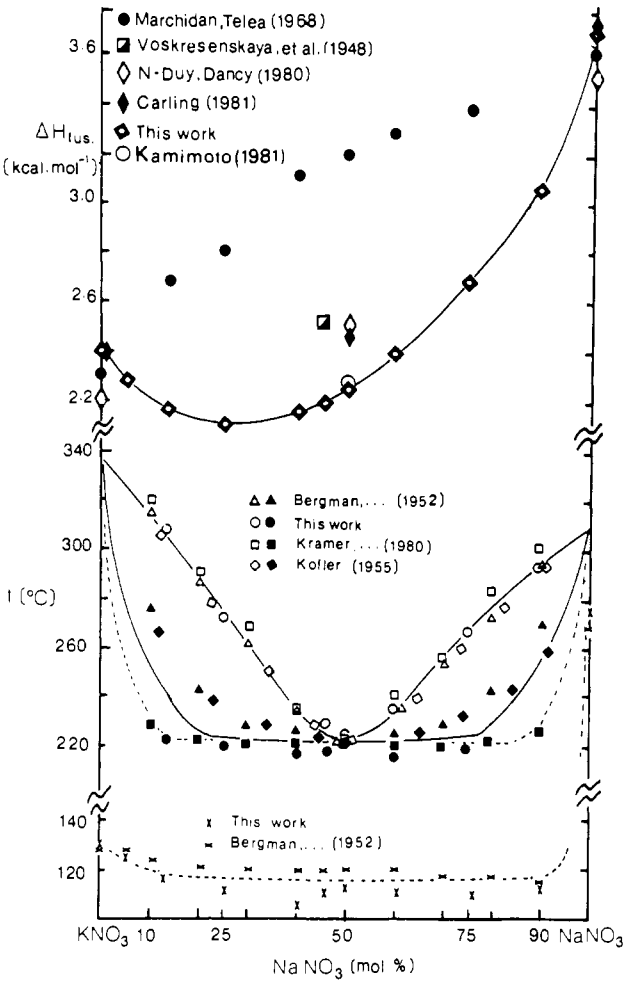

Figure 1. Variation of the enthalpy of fusion and the phase diagram for the $NaNO_3$–KNO_3 system.

were normalized to the gram-mol concept using the principles of mole fraction additivity and the molecular weights of $NaNO_3$ and KNO_3 to calculate the apparent "molecular weights" for the series of binary mixtures.

With the preceding as guidelines, the enthalpies of solid-state transitions and of melting, and the heat capacities of the materials as polycrystalline solids and in the molten (liquid) states, were determined for $NaNO_3$, KNO_3, and some 10 mixtures of intermediate compositions. The compositions of the two mixtures being evaluated in the large-scale solar energy research and development projects (*1*, *2*), namely, the equimolar mixture (or drawsalt) and the 64 mol % $NaNO_3$ mixture (i.e., 60 wt % $NaNO_3$), were included in the series thus investigated. The exact compositions and the results for the enthalpy measurements are summarized in Table I, and for the heat capacities, in Table II. The apparent molecular weights for the mixtures are included in Table I for ease in recalculating the results to unit mass as reference base. The melting temperatures (T_m) and the temperature ranges (T_{range}) were determined following the guidelines already noted (see preceding paragraph).

The composition dependence of ΔH_{fus} and the liquids–solidus lines of the phase diagram for $NaNO_3$–KNO_3 are shown in Figure 1, together with the results of the three most recent phase-diagram studies (Bergman and Berul (*8*), Kofler (*9*), and Kramer and Wilson (*10*)) and the published results for the enthalpies of melting (Marchidan and Telea (*4*), Voskresenskaya et al. (*5*), Nguyen-Duy and Dancy (*6*), and Carling (*7*)). The phase diagram for this system has been the subject of more than 20 independent investigations over the period from 1884 to the present date. For details, see Voskresenskaya (*11*). It remained for Kramer and Wilson (*10*) to define more exactly the solidus and liquidus lines in this system.

Inspection of the results (Table I and Figure 1) shows that the liquidus and solidus limits proposed by Kramer and Wilson and the solid-state transitions noted by Bergman and Berul are firmly supported by the present work. The melting point of the equimolar minimum-melting mixture, furthermore, is found to be 493 K (220 °C). This compares with 494 (Carling (*8*)), 495 (Nguyen-Duy and Dancy (*6*)), and 495 K (Bergman and Berul (*8*)). The somewhat higher value by Kramer and Wilson, 500 K, is thus questioned. In the latter study (*10*), it was shown that the experimental data for liquidus–solidus can be computer modeled from regular solution theory; for the equimolar composition, the heat of mixing for the solid solution is thus estimated to be 375 cal mol^{-1}. With some exceptions, most of the earlier investigations support the equimolar composition as that of the minimum-melting mixture (see ref *11*).

Relative to the enthalpies of fusion, the earlier results reported by Marchidan and Telea (*4*) are clearly not supported (see Figure 1). The results reported for the equimolar mixture by Nguyen-Duy and Dancy (drop calorimetry) (*6*) and Carling (DSC techniques) (*7*), and for the 46 mol % composition by Voskresenskaya et al. (drop calorimetry) (*5*), and the present results are consistently lower than the Marchidan–Telea values (*4*). In the latter study (*4*), a Calvet-type microcalorimeter was used, and, while the results for enthalpies of fusion for $NaNO_3$ and KNO_3 appear sound (3.60 and 2.30 kcal mol^{-1}, respectively), the values for the intermediate compositions fall uniformly above the present values. The difference appears to be too large for measurement errors, but there are insufficient details in the publication to sort out the contributing causes for the higher values.

Table II. Heat Capacities for $NaNO_3$–KNO_3

A. Heat Capacities cal mol^{-1} deg^{-1}

System: $NaNO_3$

state	solid					molten
T, K	330	350	400	450	560–572	580–700
C_p	24.16	25.06	27.30	29.53	34.38	34.11 (±1.4)

System: KNO_3

state	solid							molten
T, K	330	350	399	450	500	550	590	600–720
C_p	23.11	24.17	26.77	30.05	31.34	32.36	33.66	34.0_5 (±1.7)

System: $NaNO_3$–KNO_3 (50:50 mol %)

state	solid			molten
T, K	330	350	400–800	520–700
C_p	23.89	24.81	30.10	33.95 (±2.5)

System: $NaNO_3$–KNO_3 (molten state)

mol % $NaNO_3$	13	25	40	46
T_{range}, K	590–720	550–700	520–700	520–700
C_p	34.47 (±1.6)	33.89 (±1.0)	34.37 (±2.0)	33.13 (±2.0)

mol % $NaNO_3$	60	64	75
T_{range}, K	520–700	520–700	560–700
C_p	33.83 (±1.5)	34.53 (±1.8)	33.86 (±0.6)

B. Temperature-Dependence Equations

system	state	$C_p = a + bT$ a	10^3b	T_{range}, K
$NaNO_3$	crystalline	9.396	4.75	330–450
KNO_3	crystalline	5.602	53.05	333–390
	crystalline	18.437	25.80	410–590
$NaNO_3$–KNO_3 50:50 mol %	crystalline	12.638	34.55	330–380

For critical discussions of the structural and thermodynamic data for the solid-state transitions in nitrates in the open scientific literature, see Rao et al. (*12*) and Janz et al. (*13*). It is sufficient to note that the values for T_{tr} and ΔH_{tr} found in the present study for KNO_3 (403 K, 1213 cal mol^{-1}) are in accord with the results recommended by Rao (*12*) (403 K, 1200 cal mol^{-1}) and the recent work of Carling (*7*) (406 K, 1350 cal mol^{-1}). By contrast, the present results for $NaNO_3$ (549 K, 224 cal mol^{-1}) receive support from the values reported by Janz et al. (*13*) (549 K, 174 cal mol^{-1}), and the more recent work of Nguyen-Duy and Dancy (*6*) (535 K, 380 cal mol^{-1}), but differ markedly from the assessment by Rao of the earlier studies (*12*) (549 K, 1030 cal mol^{-1}), and the recently reported result of Carling (*7*) (550 K, 1056 cal mol^{-1}). Additional measurements to resolve the differences thus noted for the $\Delta H_{tr}(NaNO_3)$ are needed. For the series of binary mixtures (Table I), earlier enthalpy measurements for the solid-state transition appear to be limited to those of Carling for the equimolar minimum-melting composition. Inspection shows that the agreement is all that can be expected (i.e., Carling (*7*), 386 K, 836 cal mol^{-1}; present work (see Table I), 386 K, 751 cal mol^{-1}).

The results of the heat capacity determination (Table II) are illustrated graphically as a composite diagram in Figure 2. Heat capacity measurements for the nitrates in the polycrystalline state were limited to $NaNO_3$, KNO_3, and the equimolar minimum-melting mixture in the present work. Inspection of the results (Table II) shows that the heat capacities exhibit a modest temperature dependence ($NaNO_3$, to 450 K; KNO_3 to 590 K; and $NaNO_3$–KNO_3, to 380 K) and that for these materials in the molten state (mp to ~700 K) the heat capacities are constant, within experimental limits of accuracy. The molten-state heat capacity measurements were extended to the series

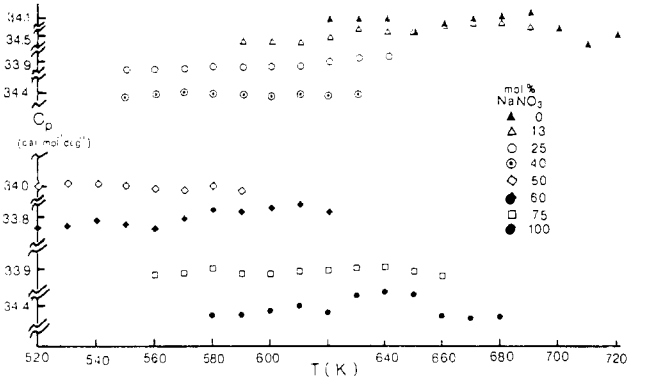

Figure 2. Heat capacities for the $NaNO_3$–KNO_3 system as a function of temperature for various compositions.

of intermediate $NaNO_3$–KNO_3 compositions. As summarized in Table II and illustrated in Figure 2, the molar heat capacities are virtually independent of composition and of temperature. The value, 34.0_5 (±2%) cal mol^{-1} deg^{-1}, may be used for the heat capacity for all compositions (including the end-members) of $NaNO_3$–KNO_3 in the molten state, from the respective melting temperatures to the upper temperature limit of the present series of measurements (see Figure 1 and Table I).

Some comparisons with the results of earlier heat capacity measurements are of interest. For $NaNO_3$–KNO_3 mixtures, the measurements appear to be limited to Nguyen-Duy and Dancy (*6*), Carling (*7*), and Voskresenskaya et al. (*5*), for the equimolar minimum-melting composition. As already noted, a marked temperature dependence, with a negative slope with

Table III. Thermal Data for $NaNO_3$-KNO_3 after Prolonged Exposure to Ambient Air Atmosphere While in the Molten State

	T_m, K	melting range, K	ΔH_{fus}, kcal mol^{-1}	C_p, cal mol^{-1} deg^{-1}	heat capacity range, K
A. $NaNO_3$-KNO_3 (50:50 mol %; minimum-melting mixture)[c]					
a	493	isothermal	2.24	33.95	600-700
b	473	459-489	1.87	34.30	600-700
B. $NaNO_3$-KNO_3 (64:36 mol % mixture)[c]					
a	518	488-518	2.43	34.53	600-700
b	498	465-498	2.16	34.46	600-700

[a] Initial values. [b] After 170 h at 600 °C, open to air. [c] Apparent molecular weights: 50:50 mol %, 93.06 g; 64.36 mol %, 90.80 g.

increasing temperatures, was reported in the latter (*5*). The marked negative temperature dependence has not been confirmed in the subsequent investigation by Carling (*7*), nor in the present work. The C_p values and temperature ranges from the latter two studies and the present work for this composition in the molten state are respectively as follows: 33.9 (±1.5%) cal mol^{-1} deg^{-1}, 495 K (*6*); 33.24 (±2%) cal mol^{-1} deg^{-1}, 500–700 K (*7*); and 33.95 (±2%) (cal mol^{-1} deg^{-1}, 520–700 K (present work; see Table II). By contrast the C_p values of Voskresenskaya et al. (*5*) for this system in the molten state decrease from 40.0 (510 K) to 33.1 (710 K) cal mol^{-1} deg^{-1}. For this system in the polycrystalline solid state, the C_p values of Voskresenskaya et al. and Carling both show a positive temperature dependence and, within the limits of experimental accuracies, are in accord with the results of the present work (refer to Table II, 50:50 mol % $NaNO_3$–KNO_3); in the study of Nguyen-Duy and Dancy (*6*), the temperature dependence may be masked by the rather large limits of accuracy assigned to the single value for this system in the solid state (±23%).

Attempts to extend to heat capacity measurements to higher temperatures proved to be unsuccessful. Above 700 K the background signal increased to a "noise" level that threw doubts on meaningful heat capacity measurements. Occasional ruptures of the crimp-seal of DSC capsules were also encountered, and these vitiated further measurements. Some limited exploratory measurements were undertaken to diagnose the source of this complication. It was shown that the molten nitrates can be contained in open (uncrimped) DSC capsules satisfactorily from T_m to temperatures approaching 700 K. In the range of ~700–720 K, a high signal noise level appears; in this range, the melt is observed to "creep" out from the sample pan and into the calorimeter pan cavity. The melt creepage is undoubtedly a manifestation of the onset of a Marigoni effect (*14*, *15*), through which the movement of the liquid, as a film, is greatly enhanced through variations in the concentrations of surface-active solute species. In the present salt system, the contributing surface-active species undoubtedly would be oxide and nitrite species arising from the decomposition of the nitrates in this temperature range. Kramer and Munir (*16*) report that such decomposition onsets in molten $NaNO_3$ and molten KNO_3 as low as 620 K. Thermal degradation studies for $NaNO_3$–KNO_3 mixtures remain an outstanding need, but it appears likely that the increased difficulties in extending the DSC technique for heat capacity measurements with molten nitrates to 700 K and higher may be attributed, in part, to such effects. In the present work, the heat capacity measurements were repeated with a fluoride melt (LiF–NaF–KF eutectic) as sample. The problems noted above with nitrates were not encountered, and the heat capacity measurements were readily extended to ~860 K.

With reference to the limited measurements undertaken to investigate the effects of prolonged exposure of the molten nitrates to ambient air atmospheres at ~600 °C (~873 K), the

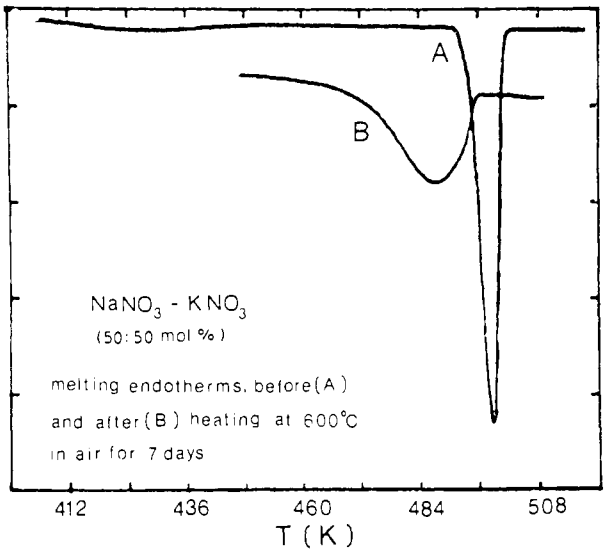

Figure 3. DSC melting endotherms for the equimolar $NaNO_3$–KNO_3 minimum-melting mixture (drawsalt) before and after prolonged exposure at 600 K to ambient air atmosphere.

results are summarized in Table III for two compositions (equimolar mixture, and 64 mol % $NaNO_3$), together with the measured values for ΔH_{fus} and C_p for these samples initially (before air exposure). Some of the features of the changes in the process of melting for the equimolar mixture are illustrated by the DSC melting endotherms in Figure 3. Chemical analyses of the samples (for nitrite and oxide content) were undertaken as part of this work. For the equimolar mixture after air exposure at 600 °C, the nitrite and oxide contents were found to be 1.62 and 2.44 mol %, respectively. (It should be noted that the ambient air atmosphere in this laboratory was one of relative low humidity.) From inspection of the results (Table III and Figure 3) it is seen that the enthalpy of fusion and especially the "process of melting" are markedly different for the air-degraded samples; by contrast the heat capacity is not significantly altered. The changes in the melting behavior are not unexpected. With decomposition to nitrites, the $NaNO_3$–KNO_3 system gains the features of the reciprocal salt system Na, K/NO_3, NO_2. The formation of carbonates can be foreseen as additional solute species through the reaction of oxides (nitrate decomposition) with atmospheric carbon dioxide. Further measurements were deferred, accordingly, until the results of studies in progress elsewhere on the interactions of molten $NaNO_3$–KNO_3 with water and carbon dioxide in the air (*17*) are available. It is sufficient to note that the changes in the measured values of ΔH_{fus} and in the nature of the melting process (summarized in Table III and Figure 3) appear to be quite sensitive criteria for the degradation of the melt composition thus induced.

The work of Kamimoto (*18*) appeared after the present communication had been submitted. As an update, the new result for the enthalpy of fusion of the 50:50 mol % $NaNO_3$–KNO_3 mixture from Kamimoto (*18*), 2.26 kcal mol^{-1}, is also shown in Figure 1. The results that we report for the heat capacities, likewise, are firmly supported.

Acknowledgment

We acknowledge with pleasure the participation of Giai Truong in the calorimetric measurements, and specifically relative to heat capacity measurements reported herewith.

Literature Cited

(1) Radosevich, L. "Thermal Energy Storage for Advanced Solar Central Receiver Power Systems"; Sandia Laboratories Report SAND 78-8221, Livermore, CA, 1978.

(2) Tallerico, L. "A Description and Assessment of Large Solar Power Systems Technology"; Sandia Laboratories Report SAND 79-8015, Livermore, CA, 1979.
(3) Janz, G. J., et al. *Natl. Stand. Ref. Data Ser. (U.S., Natl. Bur. Stand.* **1979**, *NSRDS-NBS 61*, Part II.
(4) Marchidan, D. I.; Telea, C. *Rev. Roum. Chim.* **1968**, *13*, 1291.
(5) Voskresenskaya, N. K., et al., *Zh. Prikl. Khim. (Leningrad)* **1948**, *21*, 18.
(6) Nguyen-Duy, P.; Dancy, E. A. *Thermochim. Acta* **1980**, *39*, 95.
(7) Carling, R. W. *Proc. Int. Symp. Molten Salts, 3rd*, **1981**, 485.
(8) Bergman, A. G.; Berul, S. I. *Izv. Sekt. Fiz-Khim. Anal., Inst. Obshch. Neorg. Khim., Akad. Nauk SSSR.* **1952**, *21*, 178.
(9) Kofler, A. *Montash. Chem.* **1955**, *86*, 643.
(10) Kramer, C. M.; Wilson, C. J. *Thermochim. Acta* **1980**, *42*, 253.
(11) Voskresenskaya, N. K., Ed. "Handbook of Solid-Liquid Equilibria in Systems of Inorganic Salts" (2 vols.), *Izv. Akad. Nauk SSSR.*, Moscow, 1961, Israel Program for Scientific Translation, Jerusalem, 1970; NTIS, Washington, D.C.
(12) Rao, C. N. R.; Prakash, B.; Natarajan, M. *Natl. Stand. Ref. Data Ser. (U.S.), Natl. Bur. Stand.* **1975**, *NSRDS-NBS 53*.
(13) Janz, G. J.; Kelly, F. J.; Perano, J. L. *J. Chem. Eng. Data* **1964**, *9*, 133.
(14) Scriven, L. E.; Sterling, C. V. *Nature (London)* **1960**, *187*, 186.
(15) Brimacombe, J. K.; Weinberg, F., *Metall. Trans.* **1972**, *3*, 2298.
(16) Kramer, C. M.; Munir, Z. A. *Proc. Int. Symp. Molten Salts, 3rd*, **1981**, 494.
(17) EIC Corp. *Waltham*, MA; cited by: Carling, R. W. In "Molten Nitrate Salt Technology Development Status Report"; Sandia Laboratories Report SAND 80-8052, Livermore, CA, 1981, p 14.
(18) Kamimoto, M. *Thermochim. Acta* **1981**, *49*, 319.

Received for review February 4, 1982. Accepted May 18, 1982. The DSC facility used in this work and the acquisition and design of the computer accessories were made possible, in large part, by support received from the U.S. Department of Energy, Division of Materials Research.

Vapor–Liquid Equilibrium in the System Methyl Ethyl Ketone–*p*-Xylene

Jaime Wisniak* and Abraham Tamir

Department of Chemical Engineering, Ben-Gurion University of the Negev, Beer-Sheva 84120, Israel

New vapor–liquid equilibrium data have been obtained for the binary system methyl ethyl ketone–*p*-xylene at 760 mmHg to compare with previously reported data assumed to be thermodynamically inconsistent. The system presents slight positive deviations from ideal solution behavior. The activity coefficients are well correlated by a three-constant Redlich–Kister equation and by the Wilson equation. Boiling points are adequately described by a four-constant equation, and vapor composition is very accurately predicted by the UNIFAC method.

Introduction

Chandrashekara and Seshadri (*1*) have recently reported vapor–liquid equilibria data for the system methyl ethyl ketone (MEK)–*p*-xylene and chlorobenzene–*p*-xylene at 685-mmHg pressure. They have analyzed the thermodynamic consistency of their data using the Herington criteria (*2*) based on an empirical evaluation of heats of mixing effects. On this basis, they claim that their data are consistent in spite of the fact that, for MEK concentrations of less than $X_1 = 0.35$, γ_1 is larger than unity for MEK and smaller than unity for *p*-xylene. The same behavior, although much less pronounced, is reported for the binary chlorobenzene–*p*-xylene.

The system MEK–*p*-xylene is not believed to exhibit such strong deviations from ideal solution behavior to justify the behavior observed; we believe that it is due to poor, inconsistent data and not to heat effects. We have measured the vapor–liquid equilibrium data at 760 mmHg to verify our assumptions.

No other data are available on the MEK–*p*-xylene system for further comparison.

We can mention that Burke et al. (*3*) observed the same behavior in their measurement of the vapor–liquid equilibrium of the system methanol–toluene. Further measurements by Ocon et al. (*4*) showed that the data of Burke are not reliable.

Experimental Section

Purity of Materials. Analytical-grade reagents purchased from Merck and Fluka were used without further purification after gas-chromatography analysis failed to show any significant impurities.

Table I. Physical Constants of Pure Compounds

index	compd	refractive index at 25 °C	bp(760 mmHg), °C	% purity GLC (min)
1	methyl ethyl ketone	1.378[a]	79.56[a]	99.5
		1.376[b]	79.60[b]	
2	*p*-xylene	1.494[a]	138.3[a]	99.0
		1.493[b]	138.4[b]	

[a] Measured. [b] Reference 8.

Table II. Experimental Vapor-Liquid Equilibria Data

T, °C	x_1	y_1	y_1-(UNIFAC)[a]	calcd (eq 1) γ_1	calcd (eq 1) γ_2
129.45	0.048	0.208	0.218	1.203	1.049
125.42	0.079	0.317	0.324	1.215	1.043
123.25	0.102	0.381	0.394	1.187	1.030
116.80	0.161	0.511	0.524	1.169	1.048
112.44	0.210	0.594	0.604	1.155	1.052
105.55	0.305	0.710	0.719	1.127	1.056
101.15	0.387	0.755	0.793	1.087	1.070
95.30	0.506	0.852	0.861	1.068	1.061
93.90	0.546	0.872	0.886	1.053	1.047
89.45	0.670	0.917	0.934	1.023	1.091
86.55	0.770	0.947	0.971	0.999	1.108
85.02	0.815	0.959	0.976	1.000	1.126
84.58	0.831	0.962	0.972	0.996	1.161
80.65	0.970	0.994	1.000	0.992	1.194

[a] $y_1(\text{UNIFAC}) = p^\circ_1 x_1 \gamma_1(\text{UNIFAC})/P$.

Physical properties of the pure components appear in Table I.

Apparatus and Procedure. An all-glass modified Dvorak and Boublikova recirculation still (*5*) was used in the equilibrium determinations. The experimental features have been described previously (*6*). All analyses were carried out by gas chromatography on a Packard-Becker Model 417 apparatus provided with a thermal conductivity detector and an Autolab Model 6300 electronic integrator. The column was 200 cm long and 0.2 cm diameter and was packed with SP 1200 on 80–100 Supelcoport and operated isothermally at 105 °C.

Injector temperature was 270 °C and the detector operated at 150 mA and 280 °C. Calibration analyses were carried on

0021-9568/82/1727-0428$01.25/0